



The effect of rapid relative humidity changes on fast filter-based aerosol particle light absorption measurements: uncertainties and correction schemes

Sebastian Düsing¹, Birgit Wehner¹, Thomas Müller¹, Almond Stöcker², Alfred Wiedensohler¹

5 ¹Leibniz Institute for Tropospheric Research (TROPOS), 04318 Leipzig, Germany

²Ludwig-Maximilians-University Munich, Department of Statistics, 80539 Munich, Germany

Correspondence to: Sebastian Düsing (duensing@tropos.de)

Abstract.

Measuring vertical profiles of the particle light absorption coefficient by using absorption photometers may face the
10 challenge of fast changes in relative humidity. These absorption photometers determine the particle light absorption coefficient
due to a change in light attenuation through a particle-loaded filter. The filter material, however, takes up or releases water
with changing relative humidity (rh in %), influencing thus the light attenuation.

A sophisticated set of laboratory experiments was therefore conducted to investigate the effect of fast rh changes
(drh/dt) on the particle light absorption coefficient (σ_{abs} in Mm^{-1}) derived with two absorption photometers. The rh dependency
15 was examined based on different filter types and filter loadings with respect to loading material and loading areal density. The
Single Channel Tri-Color Absorption Photometer (STAP; Brechtel Manufacturing Inc, 1789 Addison Way, Hayward, CA
94544, USA) relies on quartz-fiber filter (PALL LifeScience, Pallflex Membrane Filters Type E70-2075W) and the
microAeth® MA200 (AethLabs, 1640 Valencia St, Suite 2C, San Francisco, CA 94110, USA) is based on a
20 Polytetrafluoroethylene (PTFE) filter band. Furthermore, three cases were investigated: clean filter, filter loaded with black
carbon (BC) and filter loaded with ammonium sulfate. The filter loading areal densities (ρ^*) ranged from 3.1 to 99.6 mg m^{-2}
in the case of the STAP and ammonium sulfate, 1.2 to 37.6 mg m^{-2} considering the MA200. Investigating BC loaded cases,
 ρ^*_{BC} was in the range of 2.9 to 43.0 and 1.1 to 16.3 mg m^{-2} for the STAP and MA200, respectively. In addition, the effect of a
silica-bead based diffusion on the rh effect was investigated.

Both instruments revealed opposing responses to relative humidity changes (Δrh) with different amplitudes. The
25 STAP shows a linear dependence to relative humidity changes. The MA200 is characterized by an exponential recovery after
its filter was exposed to relative humidity changes. At a wavelength of 624 nm and for the default 60-second running average
output, the STAP reveals an absolute change in σ_{abs} per absolute change of rh ($\Delta\sigma_{\text{abs}}/\Delta rh$) of 0.14 $\text{Mm}^{-1} \%^{-1}$ in the clean case,
0.29 $\text{Mm}^{-1} \%^{-1}$ in the case of BC loaded filters, and 0.21 $\text{Mm}^{-1} \%^{-1}$ considering filters loaded with ammonium sulfate. The 60-
second running average of the particle light absorption coefficient at 625 nm measured with the MA200 revealed a response
30 of around -0.4 $\text{Mm}^{-1} \%^{-1}$ for all three cases. Whereas the response of the STAP varies over the different loading materials, in



contrast the MA200 was quite stable. The response was for the STAP in the range of $0.17 \text{ Mm}^{-1} \%^{-1}$ to $0.24 \text{ Mm}^{-1} \%^{-1}$ considering ammonium sulfate loading and in the BC loaded case $0.17 \text{ Mm}^{-1} \%^{-1}$ to $0.62 \text{ Mm}^{-1} \%^{-1}$, respectively. In the ammonium sulfate case, the minimum response shown by the MA200 was $-0.42 \text{ Mm}^{-1} \%^{-1}$ and $-0.36 \text{ Mm}^{-1} \%^{-1}$ at maximum, $-0.42 \text{ Mm}^{-1} \%^{-1}$ and $-0.37 \text{ Mm}^{-1} \%^{-1}$ in case of BC loading, respectively. Using the aerosol dryer upstream, the STAP did not
35 change the behavior, but the amplitude of the observed effect was reduced by a factor of up to three.

A linear correction function for the STAP was developed here. It is provided by correlating 1 Hz resolved recalculated particle light absorption coefficients and rh change rates. The linear response is estimated with $10.08 \text{ Mm}^{-1} \text{ s}^{-1} \%^{-1}$ and can be used to correct for bias induced to rh changes at this time resolution. A correction approach for the MA200 is also provided, however, the behavior of the MA200 is more complex. Further research and multi-instrument measurements have to be
40 conducted to fully understand the underlying processes, since the correction approach resulted in different correction parameters across various experiments. However, the exponential recovery after the filter of the MA200 experienced a rh change could be reproduced.

Due to our findings, we recommend to use an aerosol dryer upstream of absorption photometers to reduce the rh effect significantly. Furthermore, when absorption photometers are used in vertical measurements, the ascending or descending
45 speed through layers of large rh gradients has to be low to minimize the observed rh effect. Additionally, recording the rh of the sample stream allows correcting for the bias during post processing of the data. This data correction leads to reasonable results, according the given example in this study.

1 Introduction

Black carbon (BC) and its light-absorbing properties has significant influence on the Earth's climate, and its
50 contribution is associated with major uncertainties, in particular due to its vertical distribution (Zarzycki and Bond, 2010). In addition, it is suspected to affect human health (WHO, 2012). Absorption photometer are feasible instruments to measure the light absorbing properties of aerosol particles. These photometers measure the aerosol particle light absorption coefficient (σ_{abs}) by detecting the change of attenuation of light due to deposited aerosol particle mass on sample filter. They have been installed on airship platforms (Rosati et al., 2016), tethered balloon platforms (Ran et al., 2016; Ferrero et al., 2014, Ferrero et
55 al., 2016) or unmanned aircraft systems (UAS; Markowitz et al., 2017, Telg et al., 2017, Bärffuss et al., 2018) to address the vertical BC distribution. To investigate human exposure to health-harming BC-containing aerosol particles from combustion sources, they have been used for mobile measurements (Capeda et al., 2017 and references therein; Alas et al, 2018).

Subramanian et al. (2007), Vecchi et al. (2013) and Lack et al. (2008) have shown, that liquid-like brown carbon can significantly bias filter-based absorption measurements since this organic carbon wraps around filter fibers and alters their
60 structural properties. Aerosol samples contain water vapor represented by its relative humidity (rh). Similarly to the liquid-like brown carbons, during the sampling process, water vapor can be adsorbed by the filter material or might be bound on the binding material within the filters. A variety of filter materials is used in absorption photometers and the water uptake is



different across various materials. Hence, changes in the aerosol *rh* can affect the aerosol particle light absorption measurements differently. Nessler et al. (2006) has shown to which extent sudden changes in relative humidity (*rh*) can influence measurements of a Particle/Soot Absorption Photometer (PSAP; Radiance Research, Seattle, WA) and an Aethalometer for clean filter material and loaded with BC, whereas Cai et al. (2014) has shown the effect for the microAeth® AE51, however, they did not quantify it. However, hygroscopic aerosol particle species such as ammonium sulfate can take up water depending on the relative humidity. The *rh* effect for filters loaded with such aerosol species was never quantified. Furthermore, not all filter materials have been covered within these studies. Summarizing, both, filter material and loading material, may influence the light attenuation of the filter.

The *rh* effect might not be relevant for averaging periods longer than 5 minutes as usually done at stationary measurements on ground (e.g. to address human exposure to BC containing aerosol particles). However, to address vertical profiling of BC with fast *rh* changes, particle light absorption measurements require a high temporal resolution of about seconds.

Telg et al. (2017) presented a study using an unmanned aircraft system (UAS) for vertical profiling of aerosol physical properties including the aerosol particle light absorption coefficient measured by an absorption photometer. In their study, a significant decrease of σ_{abs} at around 1000 m altitude is visible. Considering the other simultaneously measured microphysical aerosol parameters, this decrease is not to be expected. In the WMO/GAW report 227 (2016), it is recommended to conduct aerosol sampling below 40% relative humidity to prevent measurements artefacts due to high relative humidity. Although the measurements of Telg et al. (2017) have been conducted following these recommendations, this is a published example for the bias in σ_{abs} measurements due to fast *rh* changes even for a *rh* below the 40% threshold.

In our study, the *rh* effect is investigated for the small-sized photometers STAP (Single Channel Tri-Color Absorption Photometer; Brechtel Manufacturing Inc, 1789 Addison Way, Hayward, CA 94544, USA), using a quartz-fiber glass filter, and MA200® (AethLabs, 1640 Valencia St, Suite 2C, San Francisco, CA 94110, USA), which relies on a Polytetrafluoroethylene (PTFE) filter. We show results of a set of laboratory experiments and address the effect of sudden changes in relative humidity for both absorption photometers. Herein, we consider three different scenarios: a) clean filters, different filter loading densities of b) hydrophobic BC, and c) hydrophilic ammonium sulfate ((NH₄)₂SO₄). In all of these cases we also investigated the impact of a silica-bead based diffusion drier to the *rh* effect.

Following scientific questions will be addressed: To which extent do STAP and MA200 are sensitive to *rh* changes, and does different loading with respect to material and areal density contribute to this effect? Can the observed effect be corrected, and which recommendations can be given for the usage of such absorption photometer? This is important because recent developments indicate that lightweight absorption measuring instruments will be used more frequently for airborne applications in the near future.



2 Experiment

95 2.1 Theory of absorption measurements

Filter-based absorption photometer measuring the decrease of intensity of light which passes through the filter-medium with a specific optical thickness. The decrease of intensity can be described quantitatively according the law of Beer-Lambert:

$$I = I_0 e^{-\sigma_{\text{ATN}}(\lambda)l}, \quad (1)$$

100 where I is the attenuated intensity of light with a wavelength λ with a raw intensity I_0 , attenuated along a path l through a medium with an light attenuation coefficient σ_{ATN} . The path length l can also be interpreted as the length of a column of aerosol passing through the sample area of the filter spot A_i of the instrument (subscript i), whereas the particles are collected and accumulated in the filter. Therefore, the path length l can be calculated by the volume, which flows at a certain rate (volume flow rate; Q_i), for a time Δt through the sample area A_i , and hence we can rewrite Eq. (1) as:

$$I(t) = I(t - \Delta t) e^{-\sigma_i(\lambda) \frac{Q_i \Delta t}{A_i f(\tau)}} \quad (2)$$

105 While aerosol particles deposit on the filter the incoming light gets additionally scattered by those particles. Hence the effective pathway of the light through the filter increases due to the multiple scattering. To account for this, in Eq. (1) $f(\tau)$ is the transmission (τ) dependent filter-loading correction factor, with:

$$\tau = \frac{I(t)}{I_0}, \quad (3)$$

110 where I_0 is the light intensity measured of for white, clean filter. For instance, Ogren (2010) published the loading correction function for the PSAP:

$$f(\tau) = (1.0796\tau + 0.71)^{-1}, \quad (4)$$

which is also used for the STAP.

Rearranging Eq. (2) gives:

$$\sigma_i(\lambda) = \ln \left(\frac{I(t)}{I(t - \Delta t)} \right) \frac{f(\tau) A_i}{Q_i \Delta t} \quad (5)$$

115 Water has a refractive index of $1.33 + i1.5e-9$ at 532 nm wavelength. Hence it interacts with incoming electromagnetic radiation. If the filter is exposed to relative humidity changes the light attenuation of the filter changes, since the water binds to the filter itself (Caroll, 1976 and Caroll, 1986). Depending on the filter material this change increases or decreases the attenuation coefficient. The hypothesis is that the change rate of the rh (drh/dt) directly determines the amplitude of change in the particle light absorption coefficient, which is directly proportional to the change of attenuation.



120 Some absorption photometer such as the STAP directly provide measurements of the aerosol particle light absorption
coefficient σ_{abs} , some, for instance the MA200, provide measurements of the equivalent black carbon (eBC; Petzold et al.
(2013)) mass concentration (M_{eBC}). eBC mass concentrations can be converted to σ_{abs} with:

$$\sigma_{\text{abs}} = M_{\text{eBC}} \cdot MAC, \quad (6)$$

in which MAC is the mass absorption cross section in $\text{m}^2 \text{g}^{-1}$.

125 Comparison of the eBC mass concentration between a MAAP (Multi Angle Absorption Photometer; Thermo Fisher
Scientific, 27 Forge Parkway, 02038 Franklin, MA, USA; Petzold and Schönlinner, 2004) at 637 nm wavelength and MA200
at 625 nm and STAP at 624 nm revealed a good agreement within 3% and within 6%, respectively. For the STAP a MAC of
6.6 $\text{m}^2 \text{g}^{-1}$ was assumed. Since a MAC of 6.6 $\text{m}^2 \text{g}^{-1}$ is used for the MAAP at 637 nm, in this study we used the σ_{abs} directly
provided by the STAP and derived with the mentioned MAC in the case for the MA200, which already accounts for multiple
130 scattering and filter loading corrections.

2.2 Instrument description

As mentioned before, we investigated two filter-based absorption photometers, which are described in the upcoming
sections. The Single Channel Tri-Color Absorption Photometer (STAP; Brechtel Manufacturing Inc, 1789 Addison Way,
Hayward, CA 94544, USA) and the MA200 (AethLabs, 1640 Valencia St, Suite 2C, San Francisco, CA 94110, USA) use
135 different filter materials. The STAP relies on a quartz-fiber glass filter, whereas the MA200 is based on a
Polytetrafluoroethylene (PTFE) filter. Since their behavior under fast changes of the relative humidity is not described yet and
we investigate both instruments in this study.

2.2.1 MA200

The microAeth® MA200 is a small sized (13.7 x 8.5 x 3.6 cm; 420g), absorption photometer measuring the
140 attenuation of light at 5 wavelengths (375, 470, 528, 625, and 880 nm; 625 nm are investigated in this study) due to deposited
particulate matter on a Polytetrafluoroethylene (PTFE) filter band. The particulate matter samples on a sample spot with 3 mm
diameter leading to a sample area of $A_{\text{spot}} \sim 0.71 \text{e-}5 \text{ m}^2$. M_{eBC} is determined under the assumption that the change of attenuation
is proportional to the deposited eBC mass. The measurements were recorded with a 1 Hz time resolution. With the DualSpot®
technology the instrument is able to reduce uncertainties related to loading effects up to 60 % (Holder et al., 2018) but was not
145 functioning at the time of the experiment.

Holder et al. (2018) reported that the measurements are slightly depending on rh and T of the aerosol sample.
However, they observed concentrations of up to 7 mg m^{-3} , at which the observed dependence on humidity and temperature did
not influence the measured values significantly. Furthermore, they used another version of the instrument (MA350), which
may react differently to changes in humidity and temperature.



150 2.2.2 Single Channel Tri-color Absorption Photometer (STAP)

The second instrument used here is the Single Channel Tri-color Absorption Photometer (STAP, Brechtel Manufacturing Inc, 1789 Addison Way, Hayward, CA 94544, USA). This photometer detects light at three wavelengths (450, 525 and 624 nm) attenuated due to particulate matter deposited on a quartz-fiber glass filter (PALL LifeScience, Pallflex Membrane Filters Type E70-2075W).

155 By default, the particle light absorption coefficient is determined internally using 60 s averages of the raw intensity measurements. Nevertheless, all raw measurements are recorded with a time resolution of 1 Hz allowing a recalculation of σ_{abs} at this time resolution. The volumetric flow is set to one liter per minute (lpm). According to the manual, at an internal averaging interval of 60 s, the measurement uncertainty is specified to 0.2 Mm^{-1} . The spot diameter is $\sim 4.8 \text{ mm}$ which leads to a sample area of $A_{\text{spot}} \sim 1.75 \text{e-}5 \text{ m}^2$.

160 2.3 Experimental Set up

The experimental setup is designed to examine the instrument filters in different states. Unloaded filters and differently loaded with black carbon and ammonium sulfate were investigated. The extent to which fast changes in the relative humidity of the air passing through the filter affect absorption measurements was investigated for these conditions.

165 A miniCAST burner (model 5200, Jing Ltd.) was used to generate soot (black carbon; BC) aerosol particles due to combustion of propane. The produced BC particles stream can be diluted according the needs of the customer. A detailed description of the miniCAST is supplied by (Jing, 1999). Additionally, a solution of ammonium sulfate ($(\text{NH}_4)_2\text{SO}_4$; solution concentration of $0.05 \text{g}/80 \text{ml}$) was nebulized to an aerosol and was dried afterwards. Either the ammonium sulfate or the BC aerosol was fed into a 0.5 m^3 stainless steel mixing chamber. A fan within the chamber ensure a well-mixed aerosol.

170 The scheme of the experimental set up is described in Figure 1. First, two particle free, dry ($\text{RH} = 0\%$) air flows were produced. One of the flows was humidified by passing two glass tubes containing distilled water at room temperature with an inlet and outlet for compressed particle free air. A maximum relative humidity of $\sim 96\%$ was reached. Both, the dry and humidified air flows were mixed together with a Swagelok brass T-shaped flow splitter and it was ensured that the sum of both mass-flows exceeded 1 lpm (controlled by a mass flow controller). Different rh were produced according to the ratios of the dry and humidified air. For this, valves with markings indicating the opening state of the valves were used to reproduce
175 consistent mixing rh . The rh and T of the airflow sampled with the photometer were detected with a temperature and relative humidity sensor (model HYT939, B+B Thermo-Technik GmbH, 78166 Donaueschingen, Germany) within an accuracy of $\pm 1.8\%$ (between 0 and 90% RH) and $\pm 0.2^\circ\text{C}$ (between 0 and 60°C). Additionally, this setup could be used with or without a silica bead-based dryer beforehand the photometers to examine to which extent a dryer dampens the effect of relative humidity changes on the photometer absorption measurements.

180 The loading aerosol was split into two streams from one of which could be sampled on the photometer filters. The other one was sampled with a mobility particle sizer spectrometer (MPSS; working principle explained in e.g. Wiedensohler



et al. (2012)) to measure the aerosol particle number size distribution. An example of a generated ammonium sulfate aerosol is shown in Figure 2. Furthermore, the mass concentration of the generated eBC (soot) was measured also with a MAAP.

3 Results

185 This chapter will give an overview of the measurement results. The overall behavior of both instruments will be shown for wavelengths of 624 nm in the case of the STAP and 625 nm in the case of the MA200, respectively. The particle light absorption coefficients in dependence of the absolute change in rh (Δrh) are the 60 second internal averaging readouts of the STAP and a 60 seconds running average considering the MA200. First, clean filters will be considered. Afterwards the behavior for loaded filters separated into BC and ammonium sulfate loading will be shown.

190 3.1 Clean filters

In Figure 3, the time series of the measured rh upstream the two photometers (upper panel) and of σ_{abs} measured by the STAP (624 nm) and MA200 (625 nm) in the lower panel are shown. The air sampled by the photometers was entirely particle-free. Relative humidity was changed in this time series between 3.1 and 87.7 %. The change rate of rh (drh/dt) was in the range of around -3.0 to 2.9 % s^{-1} . Whereas the measurements of the STAP ranging between -9.8 and 9.5 Mm^{-1} the floating
195 60 s mean of the MA200 readouts were ranging from to 32.2 to -33.6 Mm^{-1} , respectively. Furthermore, Figure 3 shows the opposing behavior of both instruments. Whereas the STAP reacts to positive change rates of the rh with positive particle light absorption coefficients, the MA200 measures negative particle light absorption coefficient and vice versa. Summarizing, this indicates that the different filter materials react opposing to each other.

Subramanian et al. (2008) observed that organic matter produced during low-temperature biomass burning has a
200 liquid, bead-shaped appearance when collected on fibrous filter. Also, these organics can appear as translucent coatings on the filter fibers and therefore change significantly the interaction with incident light. Accordingly, for this study this means that the water in the collection stream can wrap itself around the filter fibers, analogous to the organic materials. Lack et al. (2008) has estimated the bias on filter-based absorption measurement due to loading with organic material. Under conditions with low mass concentrations of organic matter the agreement with photoacoustic-based aerosol light absorption measurements was
205 12 %. Whereas under conditions where the mass concentration of organic material was 15 to 20 times larger than that of light absorbing carbon, the difference was 50 – 80 %. Therefore the effect of coating with liquid matter around the fibers is not negligible. In the case of the STAP, the water beads and coating can lead to a higher net reflectance of the filter, which appears darker for the photodiode behind the filter. The instrument interprets this as an increased attenuation and hence as an increased absorption. In addition, the backing material consists of hydrophilic cellulose, which may absorb water under increased relative
210 humidity and thus change its optical properties (Ogren et al., 2017). Compared to the fibrous structure of the quartz-fiber filter, the PTFE filter of the MA200 is a porous, hydrophobic filter. We speculate that these properties result more into a collection of a thin film of water, which could act as an index matching between the refractive indices of the PTFE and air. An additional



film with intermediate refractive index reduces the reflectance and thus increases the transmittance leading to a decreased attenuation. Hence, the instrument interprets decreases of the attenuation as negative absorption.

215 The overall behavior of both instruments in the case of clean filters is shown in Figure 4 (upper left panel). Each point represents the corresponding maximum deviation of σ_{abs} ($\Delta\sigma_{\text{abs}}$) after the rh was changed. The amplitude of the relative humidity change was estimated by subtracting the starting rh at the start of the σ_{abs} excursion from the rh at the time of the maximum σ_{abs} deviation. Ongoing this will be referred as absolute rh change (Δrh). For all investigated Δrh , the response behavior of the MA200 ($R^2 = 0.99$) is more stable than the STAP ($R^2 = 0.78$). However, the response is stronger than the
220 average response of the STAP at the presented wavelength. Whereas the STAP shows a dependency of $0.14 \text{ Mm}^{-1} \%^{-1}$, which means an increase in absorption with increasing rh , the MA200, shows an opposing behavior with a larger absolute value in the slope of $-0.41 \text{ Mm}^{-1} \%^{-1}$ (Table B 1 **Fehler! Verweisquelle konnte nicht gefunden werden.**).

3.2 Loaded filters

Different aerosol types deposit on the filter within the instruments while measuring σ_{abs} . These aerosol types are either
225 hydrophilic or hydrophobic and hence experience water uptake or not under conditions of elevated rh . Hereby, the more particle material is deposited on the filter the more water deposits on the filter. Therefore, this section will show the influence of different filter loading materials on the rh effect and will also point out the effect of different filter loading mass. Filter loading mass is calculated by multiplying the apparent loading mass concentration of the considered material with flow of the instrument and loading duration. The different sample spot areas of the absorption photometers will be considered herein by
230 normalizing the loaded mass with the respective sample spot area. Ongoing this will be referred as filter loading areal density ρ^* .

3.2.1 Black carbon

During the experiment the eBC loading mass concentration was estimated with different methods depending on the stability of the mass concentration and loading duration and was ranging between 27.6 and $52.6 \mu\text{g m}^{-3}$. In Table 1 ρ^* of eBC
235 per spot area (ρ^*_{eBC}) of both instruments is shown. Four different ρ^*_{eBC} were considered in the case of the STAP, three for the MA200, respectively. Due to the smaller volume flow rate of the MA200, ρ^*_{eBC} is in each corresponding case smaller than ρ^*_{eBC} for the STAP and therefore, if any effects of different loadings are observed these might be not as distinct as for the STAP.

For all considered BC loading cases the averaged response of STAP and MA200 to relative humidity changes is
240 shown in Figure 4 (upper right panel) and corresponding linear fitting and correlation parameters are given in Table B 1. The STAP shows a dependency of $0.29 \text{ Mm}^{-1} \%^{-1}$ in this case. This means absolute changes in rh affecting the BC loaded filter leading to stronger σ_{abs} deviations than in the clean case. For the MA200, the response of the instrument to rapid changes in rh does not depend on the loading material the filter with BC since the regression slope is the same as in the clean case. However, the y-intersects deviate from each other but within 0.6 Mm^{-1} . We assume that this could be due to the lower absolute loading



245 on the filter (15% of the STAP loading because of 0.15 lpm flow rate compared to 1 lpm of the STAP) or the MA200 response is in general independent of the filter loading material.

Considering different loading areal densities, the MA200 shows more or less the same behavior (see Table B 1 and Figure 6). The slope of the linear correlation fit ranges from $-0.42 \text{ Mm}^{-1} \%^{-1}$ to $-0.37 \text{ Mm}^{-1} \%^{-1}$ for corresponding loading areal densities of 1.1 to 16.3 mg m^{-2} . The STAP shows a larger variability (Figure 6, left panel, black and gray colors). For ρ^* of 2.8 to 42.9 mg m^{-2} the STAP response ranges from $0.17 \text{ Mm}^{-1} \%^{-1}$ to $0.62 \text{ Mm}^{-1} \%^{-1}$. However, these results may not be entirely representative since R^2 is only for a loading density of 13.7 mg m^{-2} larger than 0.9 (0.94). Maybe the smaller amount of data points in the other cases explains this. However, the number of data points observed with the MA200 was also small but R^2 is in each case larger than 0.9.

3.2.2 Ammonia sulfate

255 The mass of the deposited $(\text{NH}_4)_2\text{SO}_4$ aerosol was estimated by integrating the aerosol particle volume size distribution of the generated ammonium sulfate particles and multiplying the volume of the ammonium sulfate aerosol during the loading period (see Table 2) with an assumed ammonium sulfate density of 1.77 g cm^{-3} (Haynes, 2014). The loading mass concentrations were in the range of 27.2 to $59.3 \mu\text{g m}^{-3}$ (see Table 2).

In the experiments ammonium sulfate filter loading areal densities were 3.1 to 99.6 mg m^{-2} in the case of the STAP and 1.2 to 15.9 mg m^{-2} in the case of the MA200. Exemplarily, PNSD and PVSD of the ammonium sulfate aerosol of the loading on Feb. 23 are shown in Figure 2. It is clearly visibly that the ammonium maximum in the particle volume size distribution peaked around a mobility diameter of 260 nm .

Figure 5 shows exemplarily the time series of the sample air rh and of the σ_{abs} measured with STAP and MA200. A rh of 0.0 to 96.2% with humidity change rates of -1.42 to 1.09 \% s^{-1} was measured. Compared the case in Figure 3 here a step-wise change of rh is shown. These steps resulted in a smaller absolute excursion of σ_{abs} which ranges from -7.2 to 9.0 Mm^{-1} (STAP; 624 nm , 60 s measurement resolution) and -14.1 to 10.9 Mm^{-1} (MA200; 625 nm , 60 second running mean).

In Figure 4 (lower left panel), the overall response of both instruments to rh changes is shown in the case of loading with ammonium sulfate. The MA200 behaves similarly to the clean and BC case (slope of $-0.40 \text{ Mm}^{-1} \%^{-1}$). The σ_{abs} measured by the STAP responses opposing with a positive slope of $0.21 \pm 0.01 \text{ Mm}^{-1} \%^{-1}$ which is roughly half the amplitude shown by the MA200 and around two thirds of the BC loaded case.

It seems that for the STAP the slope of the correlation increases with increasing imaginary part of the loading material ($0.15 \text{ Mm}^{-1} \%^{-1}$ for a clean filter, $0.21 \text{ Mm}^{-1} \%^{-1}$ for ammonium sulfate with an imaginary part of $i0.002 \pm 0.002$ (at 532 nm Dinar et al, 2007) or $i6.361\text{e-}8$ (at 550 nm and $40 \text{ \% } rh$; Erlick et al, 2011), and $0.30 \text{ Mm}^{-1} \%^{-1}$ for BC with an imaginary part of $i0.65$ at 530 nm (Kim et al., 2015 following Ackermann and Toon (1981))). Three different cases were observed in this study only so that more materials should be considered to confirm or neglect this theory.

No correlation of linear regression slope and filter loading areal density ρ^* was observed in either case, for the STAP and the MA200, respectively. The slope (a) of STAP ranges from $0.17 \text{ Mm}^{-1} \%^{-1}$ to $0.24 \text{ Mm}^{-1} \%^{-1}$, and from $-0.36 \text{ Mm}^{-1} \%^{-1}$



to $-0.42 \text{ Mm}^{-1} \%^{-1}$ for the MA200. With a relative difference from minimum to maximum slope of 15.2 % the response of the MA200 is less variable than of the STAP with a relative variability of 28.6 % (slopes with $R^2 < 0.8$ excluded, all points included
280 36.8%). In Figure 6 (middle panel), the spread of the slopes within the shown cases is exemplarily shown for the investigated minimum and maximum load of the filters.

3.3 Effect with and without dryer

Drying the aerosol before sampling with an absorption photometer reduces the unrealistic response to rapid relative humidity changes (Cai et al., 2014). In Figure 7 the response of the STAP to rapid relative humidity changes is shown for the
285 case of drying the air stream beforehand (black dot) and not (red dots). The upper left panel shows all data points, whereas the upper right, lower left and lower right panel show the response in the BC, ammonium sulfate and clean case, respectively. No MA200 was available during this part of the experiment, therefore only the response of the STAP was investigated for an internal averaging period of 60 s.

The use of silica-bead-based dryer reduced the excursion of σ_{abs} . Considering all data-points, the response (slope of
290 linear regression fit) is $0.19 \text{ Mm}^{-1} \%^{-1}$. Extreme amplitudes are significantly reduced by a factor of up to 3 with the used dryer. In the non-dried case (black empty dots, Figure 7) the excursion has a 2-o-98% percentile range from -9.6 to 14.5 Mm^{-1} (-2.4 to 2.7 Mm^{-1} interquartile range) whereas in the dried case we observed a 2-to-98% percentile range from -3.7 to 4.8 Mm^{-1} (-2.2 to 2.9 Mm^{-1} interquartile range). In the here presented cases the dryer was capable to reduces the difference between start and end rh by a factor of 2.4. In the non-dried case a Δrh of -80.4 to 79.8% was observed, whereas a Δrh of -34.9 to 33.1%
295 was observed in the dried case. Conclusively, when a dryer is used, for an absolute change of rh (Δrh) within the same time interval the change rate of rh (drh/dt) is smaller, which leads to a slower change in the optical properties of the filter and hence to a smaller σ_{abs} . A similar behaviour can also be observed for the clean, the ammonium sulfate, and the BC case. For all observed loading materials, the dried-case observations matching with the linear regression fit, which includes both, the dried and non-dried cases, respectively. This means, the dryer does not change the response behaviour of the STAP but clearly
300 reduces its amplitude.

3.4 Correction approach

The above chapters describe the overall behaviour of the instruments to relative humidity changes averaging time of for 60 seconds. To correct for the described effect 1 Hz time resolution is needed to resolve the instantaneous response of the instruments to relative humidity changes. For this purpose, a further laboratory experiment was conducted in which the inlets
305 of both instruments could be flexibly exposed to humidified air. In our particular case, we hold the inlet into a beaker with a moistened tissue. In order to avoid bias by a filter, all measurements were conducted under relatively clean laboratory conditions with a background of about σ_{abs} of 1.2 Mm^{-1} . First we will consider the STAP and afterwards the MA200 is investigated.



3.4.1 STAP

310 In Figure 8 the correlation of rh change rate (drh/dt) and the measured σ_{abs} at 624 nm measured by the STAP (red circles) and recalculated with respect to standard conditions (pressure of 1013.25 hPa and temperature 273.15 K) is shown. The STAP-based background eBC mass concentration during the experiment was $\sim 190 \text{ ng m}^{-3}$ (at standard conditions, σ_{abs} at 624 nm converted with a MAC of $6.6 \text{ m}^2 \text{ g}^{-1}$), which corresponds to offset (standard conditions corrected values) in the shown scatterplot of Figure 8 and which has no influence on the response to rh changes as shown previously.

315 The rh change rate ranged from -10.8 to 14.5 \% s^{-1} . These rates correspond to a σ_{abs} of -231 to 192 Mm^{-1} for recalculated values at standard conditions and -203 to 164 Mm^{-1} directly measured by the instrument. On average the slope (correction factor C_{rh} in Eq. (7)) of the linear fit is $10.08 (\pm 0.12) \text{ Mm}^{-1} \text{ s \%}^{-1}$ for standard conditions and $8.82 (\pm 0.10) \text{ Mm}^{-1} \text{ s \%}^{-1}$ for direct instrument output, respectively. Calculating the particle light absorption coefficient introduced by rh changes $\sigma_{\text{abs,rh}} = C_{\text{rh}} \cdot drh/dt$ for different rh change rates in both, the recalculated and direct instrument output case, and subtracting it
320 from measurements allows to correct for the observed effect as follows:

$$\sigma_{\text{abs,corr}} = \sigma_{\text{abs,meas}} - C_{\text{rh}} \frac{drh}{dt}. \quad (7)$$

The y-intersect of the linear fit in Figure 8 has not to be considered for correction as mentioned before. The upper function can be applied since the STAP instantaneously reacts to rh changes and immediately shows the unbiased σ_{abs} , when no change in rh is prevalent. Disadvantageously, with this correction the noise of the rh sensor will propagate in the corrected
325 σ_{abs} . Furthermore, the linear fit in Figure 8 under- or overestimates the behavior in regimes of very high relative humidity change rates, so that in these cases the correction function cannot entirely correct the bias. Furthermore, since only one STAP was tested, other STAP may have other correction factors due to unit to unit variability. Additionally, other filter materials used in the STAP can also lead to another behavior.

Exemplarily, Figure 9 shows the application of the correction function for STAP measurements. The figure shows
330 airborne measurements of σ_{abs} at 624 nm derived with the STAP derived during a campaign conducted in March 2017 in East Germany. The upper panel displays the rh of a dried aerosol sample stream measured upstream of the STAP. The lower panel shows the recalculated σ_{abs} at 624 nm wavelength corrected for rh changes (black) and biased by rh changes (red). In the periods where the rh changes relatively fast (drh/dt of -0.55 to 0.56 \% s^{-1} e.g. at around 6200 seconds), the uncorrected σ_{abs} overshoots. The correction significantly reduces this bias and smooth out the measurements during the periods of rh changes.
335 At the peaks of drh/dt the difference of the corrected and uncorrected values is up to 1.5 Mm^{-1} , which is significant with respect to the measured σ_{abs} . The periods with negative σ_{abs} are not introduced by the rh effect. We moreover think that a small offset is introduced in the initialization process of the instrument.



3.4.2 MA200

Whereas the STAP shows a linear response to rh changes, the MA200 is more complex and shows an exponential decay after it got exposed to rh changes. Therefore, the particle light absorption coefficient can be described as a function of drh/dt at a given time t ($\sigma_{abs,rh,t}$):

$$\sigma_{abs,rh,t} = a \frac{drh}{dt} + b\sigma_{abs,rh,t-1}, \quad (8)$$

with a is a linear factor describing the dependency of $\sigma_{abs,rh}$ to drh/dt and b is an exponential decay parameter between 0 and 1. The Eq. (8) corresponds to an autoregressive moving average model with exogenous variable (ARMA-X).

The function *marima* of the R package *marima* (v2.2) is capable to derive such an ARMA-X model (details in Appendix A). From this the coefficients a and b can be derived. These can be furthermore used as initial parameters for an optimization by minimizing the sum of the squared residual errors. The derived ARMA-X model describes $\sigma_{abs}(drh/dt)$ as follows:

$$\sigma_{abs,rh}(t) = -0.47 \left[\frac{Mm^{-1}s}{\%} \right] \frac{drh}{dt}(t) + 0.93\sigma_{abs,rh}(t-1), \quad (9)$$

and with the applied optimization:

$$\sigma_{abs,rh}(t) = -0.50 \left[\frac{Mm^{-1}s}{\%} \right] \frac{drh}{dt}(t) + 0.96\sigma_{abs,rh}(t-1). \quad (10)$$

Figure 10 shows time series of rh (upper panel) and 60 s floating average σ_{abs} derived with the MA200 at 625 nm with 1 Hz time resolution derived during the laboratory experiment mentioned in 3.4. Under the influence of drh/dt in the range of -11.2 to 17.1 % s^{-1} the 60 s floating average of σ_{abs} is between -6.5 to 7.7 Mm^{-1} (M_{eBC} equivalent of -0.99 to 1.20 $\mu g m^{-3}$). Subtracting the calculated particle light absorption coefficient in dependency of rh changes following Eq. (9) and (10) to this data set σ_{abs} shrinks to -3.2 to 4.7 Mm^{-1} or -1.0 to 3.7 Mm^{-1} in the non- and optimized case, respectively. This corresponds to M_{eBC} of around -0.5 to 0.7 $\mu g m^{-3}$, or -0.2 to 0.6 $\mu g m^{-3}$ in the optimized case. This indicates, that the presented approach can significantly reduce the rh bias in the presented case. But, rh change induced fluctuations in σ_{abs} are still visible, which indicates that correction scheme cannot account entirely for all the bias introduced by a change in rh .

Unfortunately, the application of the same correction approach to other similar experiments resulted in different correction function a and b . Applying the approach to two clean case experiments from section 3.1 resulted in optimized parameters of $a = -0.92$ and -1.03 and $b = 0.974$ and 0.971 , respectively. Hence, it is just a first step trying to account for relative humidity changes and further research with more MA200 simultaneously has to be done to fully understand the underlying processes. Nevertheless, the presented approach significantly reduces the amplitude of the bias in the shown data set (see Figure 10). But, up to now we cannot recommend to use the given parameters to correct for rh effects.



6 Summary and Conclusion

Here we presented a unique set of laboratory studies to investigate the response of two different types of filter-based absorption photometers (STAP and MA200) with different filter material (quartz-fiber glass, and PTFE) to relatively fast changes in relative humidity of sampled aerosol. Different filter loading densities with different loading material (clean, black carbon, and ammonium sulfate) were considered in this study. Both instruments revealed that they react to fast humidity changes but in opposite ways, induced by the different filter material. No significant differences between the loading aerosol types were observed in the case of the MA200, whereas the STAP revealed the strongest response in the BC case. Furthermore, we investigated the effect of drying the airstream (aerosol) beforehand. Installing a dryer upstream reduced the excursion significantly, because the absolute excursion of the prevalent σ_{abs} was reduced more than two times in amplitude.

The MA200 revealed a very robust response of -0.42 to $-0.36 \text{ Mm}^{-1} \%^{-1}$ (negative excursion of σ_{abs} with increasing rh), whereas the STAP was more fluctuating across loading areal density and loading aerosol type with a positive excursion of σ_{abs} in the range of 0.17 to $0.62 \text{ Mm}^{-1} \%^{-1}$. We assume that in the case of the MA200 it is more a filter effect, or the filter loadings were too low to have a significant effect due to the lower volume flow rate. For the STAP, more parameters could also have an effect and further investigation is needed. For loading areal density on the filter no correlation was found, although we expected that the hygroscopic ammonium sulfate will affect the transmissivity of the filter-aerosol layer. Hence, we think excursions of σ_{abs} due to relative humidity changes is mainly caused by water vapor filter material interactions and is independent of the filter loading areal density or they were too low to observe significant effects.

Furthermore, we developed some correction approaches for both instruments to account for fast rh changes. For the STAP a linear correction function could be provided. This correction follows a linear approach including a correction factor of $C_{rh} = 10.08 \pm 0.12 \text{ Mm}^{-1} \text{ s} \%^{-1}$ for standard conditions and $8.82 \pm 0.10 \text{ Mm}^{-1} \text{ s} \%^{-1}$ for direct instrument output without any corrections. Exemplarily, this correction was applied to an airborne data set and has shown promising results. For the MA200 no linear correction function can be provided, since after an excursion of σ_{abs} the MA200 shows an exponentially behaving recovery function. Therefore an ARMA-X model was developed to account for this exponential decay and to describe the σ_{abs} in dependency of drh/dt . Applying this to the presented data set, this significantly reduced the excursion introduced by rh changes. But, the presented approach cannot be applied yet and has to be derived on the base of more experiments to fully understand the underlying processes.

Recommendations

The findings summarized above lead to following recommendations how to use this type of instruments:

1. When used for vertical profiling, apparent sharp gradients in rh during the profile have to be taken into account.
 - a. For instance, the ascending speed of the profiling platform should be reduced to decrease the temporal change of rh , or



- 400
- 405
- b. when fast relative humidity changes cannot be avoided, such periods have to be removed from the data set, or have to be corrected with the provided correction functions.
 2. The usage of a dryer is highly recommended, because it reduces the amplitude of the excursion in the measurements during fast *rh* changes.
 3. With or without a dryer used beforehand, we recommend recording the *rh* and *T* of the sampled aerosol. This allows to determine *rh* change rates, which then can be used to correct the biased σ_{abs} due to changes in relative humidity with the provided correction function. In the case of MA200 the presented correction approach has to be refined on the basis of more measurements to provide a useful correction function.



Appendix A: Multivariate Autoregressive Integrated Moving Average model with exogenous variable – MARIMA-X

The multivariate autoregressive integrated moving average model with exogenous variable (MARIMA-X(p,d,q)) can model the behaviour of an observation driven by an exogenous variable. It consists of three parts, the autoregressive (AR) part of order p , the moving average (MA) part of order q , and the integrating (I) part, which describes how often (d times) a time series must be differentiated to be stationary. An MARIMA-X model can be described as:

$$Y_t = aX_t + b_1Y_{t-1} + b_2Y_{t-2} + \dots + b_nY_{t-n} + \epsilon_t + c_2\epsilon_{t-2} + c_1\epsilon_{t-1} + \dots + c_n\epsilon_{t-n}, \quad (\text{A1})$$

with Y_t the predicted value of the model at the time t . b_1Y_{t-1} to b_nY_{t-n} are part of the autoregressive module of the model, with the corresponding coefficients b_1 to b_n , describing the contribution of each Y_{t-n} to Y_t . X_t represents the corresponding independent exogenous variable at time t , whereas the ϵ_t are part of the moving average of the model, which accounts for lagged error terms, ϵ_t introduced by the model itself. c_1 to c_n indicate the contribution of ϵ_t to ϵ_{t-n} to Y_t . For predictions of a variable the error term is unknown. A special case of the MARIMA-X model is the MARMA-X model or ARMA-X, in which the integrating part has an order of 0. Detailed information about ARIMA models can be found in Durbin and Koopman (2012) and Lütkepohl (2005). A tutorial to estimate MARIMA models in R is provided by Spliid (2016).



420 Appendix B: Table with overview of all investigated cases

Table B 1: Coefficients of the linear regression of the instrument response to rh changes (a is slope, b is y-intersect, and R^2 the correlation coefficient) for the clean, ammonium sulfate and BC case for different loading areal densities ρ^*_i . The number of data-points is represented by n . Bold written entries represent cases with a R^2 larger than 0.8. σ indicates the standard deviation of the fitting parameters. For ammonium sulfate τ not considered.

loading aerosol	device	ρ^*_i [mg m ⁻²]	τ	n	a [Mm ⁻¹ % ⁻¹]	$\sigma(a)$ [Mm ⁻¹ % ⁻¹]	b [Mm ⁻¹]	$\sigma(b)$ [Mm ⁻¹]	R^2
clean	MA200 (625 nm)	-	-	147	-0.41	0.00	-0.28	0.10	0.99
	STAP (624 nm)	-	-	241	0.14	0.00	0.44	0.12	0.79
BC	MA200 (625 nm)	1.1	0.98	18	-0.42	0.02	0.11	0.18	0.97
		5.3	0.95	9	-0.40	0.03	0.38	0.24	0.96
		16.3	0.82	9	-0.37	0.03	0.54	0.24	0.95
	MA200 (625 nm, all)	-	-	36	-0.41	0.01	0.28	0.12	0.96
	STAP (624 nm)	2.8	0.93	13	0.17	0.05	0.14	0.52	0.47
		13.7	0.78	33	0.29	0.01	1.26	0.37	0.94
		14.0	0.74	10	0.38	0.19	0.89	1.49	0.25
		42.9	0.52	10	0.62	0.32	1.64	2.54	0.23
	STAP (624 nm, all)	-	-	66	0.29	0.02	1.00	0.48	0.72
	(NH ₄) ₂ SO ₄	MA200 (625 nm)	1.1	-	9	-0.38	0.04	0.39	0.31
4.0			-	10	-0.42	0.04	0.00	0.27	0.94
8.0			-	41	-0.41	0.01	0.10	0.13	0.97
11.9			-	10	-0.40	0.03	-0.21	0.24	0.95
12.4			-	15	-0.39	0.01	0.25	0.16	0.99
15.5			-	9	-0.37	0.03	0.47	0.23	0.95
15.9			-	18	-0.42	0.02	0.07	0.20	0.98
37.6			-	15	-0.36	0.02	0.04	0.21	0.97
MA200 (625 nm, all)		-	-	127	-0.40	0.01	0.10	0.07	0.97
STAP (624 nm)		3.1	-	10	0.17	0.09	0.35	0.72	0.23
		10.5	-	10	0.19	0.09	0.33	0.72	0.28
		21.1	-	34	0.20	0.04	0.73	0.49	0.42
		28.9	-	90	0.23	0.01	0.92	0.34	0.81
		31.3	-	10	0.19	0.09	0.34	0.71	0.28
		32.5	-	13	0.19	0.02	0.35	0.36	0.82
		40.8	-	10	0.21	0.10	0.42	0.79	0.28
		41.9	-	16	0.20	0.05	0.16	0.64	0.47
		69.8	-	56	0.19	0.01	0.89	0.16	0.96
		98.7	-	14	0.24	0.03	0.28	0.39	0.86
	99.6	-	33	0.19	0.01	0.87	0.24	0.95	
STAP (624 nm, all)	-	-	296	0.21	0.01	0.71	0.14	0.82	



425 **Acknowledgements**

We would like to thank Dr. Sascha Pfeiffer very much for his guidance in setting up the experiment and for the introduction to the particle generators. We would also like to express our sincere thanks to Ralf Käthner for his valuable support with data acquisition troubleshooting.



References

- 430 Ackerman, T. P., and Toon, O. B.: Absorption of Visible Radiation in Atmosphere Containing Mixtures of Absorbing and Non-Absorbing Particles, *Appl. Opt.*, 20, 3661–3668, 1981.
- Alas, H.D., Müller, T., Birmili, W., Kecorius, S., Cambaliza, M.O., Simpas, J.B.B., Cayetano, M., Weinhold, K., Vallar, E., Galvez, M.C. and Wiedensohler, A.: Spatial characterization of black carbon mass concentration in the atmosphere of a Southeast Asian megacity: An air quality case study for Metro Manila, Philippines. *Aerosol Air Qual. Res.* 18: 2301–2317, 2018.
- 435 Bärfuss, Konrad; Pätzold, Falk; Altstädter, Barbara; Kathe, Endres; Nowak, Stefan; Bretschneider, Lutz; Bestmann, Ulf; Lampert, Astrid: New Setup of the UAS ALADINA for Measuring Boundary Layer Properties, *Atmospheric Particles and Solar Radiation*. In: *Atmosphere* 9, p. 28, 2018.
- 440 B+B Thermo-Technik GmbH, HYT-939 data-sheet, url: https://shop.bb-sensors.com/out/media/Datasheet_digital_humidity_sensor_HYT939.pdf, 2015
- 445 Birmili, W., Weinhold, K., Rasch, F., Sonntag, A., Sun, J., Merkel, M., Wiedensohler, A., Bastian, S., Schladitz, A., Löschau, G., Cyrys, J., Pitz, M., Gu, J., Kusch, T., Flentje, H., Quass, U., Kaminski, H., Kuhlbusch, T. A. J., Meinhardt, F., Schwerin, A., Bath, O., Ries, L., Gerwig, H., Wirtz, K., and Fiebig, M.: Long-term observations of tropospheric particle number size distributions and equivalent black carbon mass concentrations in the German Ultrafine Aerosol Network (GUAN), *Earth Syst. Sci. Data*, 8, 355-382, <https://doi.org/10.5194/essd-8-355-2016>, 2016.
- 450 T. C. Bond, S. J. Doherty, D. W. Fahey, P. M. Forster, T. Berntsen, B. J. DeAngelo, M. G. Flanner, S. Ghan, B. Kärcher, D. Koch, S. Kinne, Y. Kondo, P. K. Quinn, M. C. Sarofim, M. G. Schultz, M. Schulz, C. Venkataraman, H. Zhang, S. Zhang, N. Bellouin, S. K. Guttikunda, P. K. Hopke, M. Z. Jacobson, J. W. Kaiser, Z. Klimont, U. Lohmann, J. P. Schwarz, D. Shindell, T. Storelvmo, S. G. Warren, C. S. Zender (2013), Bounding the role of black carbon in the climate system: A scientific assessment, *J. Geophys. Res. Atmos.*, 118, 5380–5552, doi:10.1002/jgrd.50171, 2013.
- 455 Cai, J., Yan, B., Ross, J., Zhang, D., Kinney, P. L., Perzanowski, M. S., Chillrud, S. N.: Validation of microAeth® as a black carbon monitor for fixed-site measurement and optimization for personal exposure characterization. *Aerosol and Air Quality Research*, 14(1), 1–9. <https://doi.org/10.4209/aaqr.2013.03.0088>, 2014.
- 460



- Carroll, B. J.: The accurate measurement of contact angle, phase contact areas, drop volume, and Laplace excess pressure in drop-on-fiber systems, *J. Coll. Interface Sci.*, 57(3), 488-495, 1976.
- Carroll, B. J.: Equilibrium conformations of liquid drops on thin cylinders under forces of capillarity. A theory for the roll-up
465 process., *Langmuir*, 2(2), 248-250, 1986.
- Cepeda, M., Schoufour, J., Freak-Poli, R., Koolhaas, C., Dhana, K., Bramer, W. and Franco, O.: Levels of ambient air pollution according to mode of transport: a systematic review. *The Lancet Public Health*, 2(1), pp.e23-e34, 2017.
- Dinar, E., Abo Riziq, A., Spindler, C., Erlick, C., Kiss, G., & Rudich, Y.: The complex refractive index of atmospheric and
470 model humic-like substances (HULIS) retrieved by a cavity ring down aerosol spectrometer (CRD-AS), *Faraday Discussions*, 137, 275-295, <https://doi.org/10.1039/b703111d>, 2007.
- Durbin, J. and Koopman, S.: Time series analysis by state space methods. Oxford: Oxford University Press, 2012.
- 475 Erlick, C., Abbatt, J. P. D., & Rudich, Y.: How Different Calculations of the Refractive Index Affect Estimates of the Radiative Forcing Efficiency of Ammonium Sulfate Aerosols. *Journal of the Atmospheric Sciences*, 68(9), <https://doi.org/10.1175/2011JAS3721.1>, 2011.
- Ferrero, L., Castelli, M., Ferrini, B. S., Moscatelli, M., Perrone, M. G., Sangiorgi, G., D'Angelo, L., Rovelli, G., Moroni, B.,
480 Scardazza, F., Močnik, G., Bolzacchini, E., Petitta, M., and Cappelletti, D.: Impact of black carbon aerosol over Italian basin valleys: high-resolution measurements along vertical profiles, radiative forcing and heating rate, *Atmos. Chem. Phys.*, 14, 9641-9664, <https://doi.org/10.5194/acp-14-9641-2014>, 2014
- Ferrero, L., Cappelletti, D., Busetto, M., Mazzola, M., Lupi, A., Lanconelli, C., Becagli, S., Traversi, R., Caiazzo, L., Giardi,
485 F., Moroni, B., Crocchianti, S., Fierz, M., Močnik, G., Sangiorgi, G., Perrone, M. G., Maturilli, M., Vitale, V., Udisti, R., and Bolzacchini, E.: Vertical profiles of aerosol and black carbon in the Arctic: a seasonal phenomenology along 2 years (2011–2012) of field campaigns, *Atmos. Chem. Phys.*, 16, 12601-12629, <https://doi.org/10.5194/acp-16-12601-2016>, 2016.
- Haynes, W.M. (ed.). *CRC Handbook of Chemistry and Physics*. 95th Edition. CRC Press LLC, Boca Raton: FL 2014-2015,
490 2014.
- Holder, A., B. Seay, A. Brashear, T. Yelverton, J. Blair, and S. Blair. Evaluation of a multi-wavelength black carbon sensor, 10th International Aerosol Conference, St. Louis, MO, September 02 - 07, 2018.



- 495 IPCC: Cubasch, U., D. Wuebbles, D. Chen, M.C. Facchini, D. Frame, N. Mahowald and J.-G. Winther: Introduction. In: Climate Change 2013: The Physical Science Basis. Contribution of Working Group I to the Fifth Assessment Report of the Intergovernmental Panel on Climate Change [Stocker, T.F., D. Qin, G.-K. Plattner, M. Tignor, S.K. Allen, J. Boschung, A. Nauels, Y. Xia, V. Bex and P.M. Midgley (eds.)]. Cambridge University Press, Cambridge, United Kingdom and New York, NY, USA, 119–158, doi:10.1017/CBO9781107415324.007., 2013.
- 500
- Jing, L.: Standard Combustion Aerosol Generator for Calibration Purposes. 3rd ETH Conference on Combustion Generated Nanoparticles. Zurich, 9–10 August, 1999.
- Kim, J., Bauer, H., Dobovičnik, T., Hitzenberger, R., Lottin, D., Ferry, D., & Petzold, A.: Assessing optical properties and refractive index of combustion aerosol particles through combined experimental and modeling studies. *Aerosol Science and Technology*, 49(5), 340-350, <https://doi.org/10.1080/02786826.2015.1020996>, 2015.
- 505
- Lack, D. A., Cappa, C. D., Covert, D. S., Baynard, T., Massoli, P., Sierau, B., Bates, T. S., Quinn, P. K., Lovejoy, E. R., & Ravishankara, A. R.: Bias in Filter-Based Aerosol Light Absorption Measurements Due to Organic Aerosol Loading: Evidence from Ambient Measurements, *Aerosol Science and Technology*, 42:12, 1033-1041, DOI: 10.1080/02786820802389277, 2008.
- 510
- Lütkepohl H.: *Introduction To Multiple Time Series Analysis*, Berlin: Springer-Verlag; 2005.
- Markowicz, K. M., Ritter, C., Lisok, J., Makuch, P., Stachlewska, I. S., Cappelletti, D., Chilinski, M. T.: Vertical variability of aerosol single-scattering albedo and equivalent black carbon concentration based on in-situ and remote sensing techniques during the iAREA campaigns in Ny-Ålesund. *Atmospheric Environment*. <https://doi.org/10.1016/j.atmosenv.2017.06.014>, 2017.
- 515
- Nessler, R., Sheridan, P.J., Ogren, J.A., Weingartner, E., and Hannemann, A.: Effect of humidity on filter-based measurements of the aerosol light absorption. NOAA ESRL GLOBAL MONITORING ANNUAL CONFERENCE, 2006.
- 520
- Ogren, J. A., Wendell, J., Andrews, E., and Sheridan, P. J.: Continuous light absorption photometer for long-term studies, *Atmos. Meas. Tech.*, 10, 4805-4818, <https://doi.org/10.5194/amt-10-4805-2017>, 2017.
- 525
- Ogren, J.A.: Comment on “Calibration and Intercomparison of Filter-Based Measurements of Visible Light Absorption by Aerosols”, *Aerosol Science and Technology*, 44:8, 589-591, DOI: 10.1080/02786826.2010.482111, 2010.



- Petzold, A. and M. Schönlinner: Multi-angle absorption photometry – a new method for the measurement of aerosol light absorption and atmospheric black carbon, *J. Aerosol Sci.*, 35, 421-441, 2004.
- 530
- Petzold, A., Ogren, J. A., Fiebig, M., Laj, P., Li, S.-M., Baltensperger, U., Holzer-Popp, T., Kinne, S., Pappalardo, G., Sugimoto, N., Wehrli, C., Wiedensohler, A., and Zhang, X.-Y.: Recommendations for reporting "black carbon" measurements, *Atmos. Chem. Phys.*, 13, 8365-8379, <https://doi.org/10.5194/acp-13-8365-2013>, 2013.
- 535
- Ran, L., Deng, Z., Xu, X., Yan, P., Lin, W., Wang, Y., Tian, P., Wang, P., Pan, W., and Lu, D.: Vertical profiles of black carbon measured by a micro-aethalometer in summer in the North China Plain, *Atmos. Chem. Phys.*, 16, 10441–10454, <https://doi.org/10.5194/acp-16-10441-2016>, 2016.
- Rosati, B., Herrmann, E., Bucci, S., Fierli, F., Cairo, F., Gysel, M., Tillmann, R., Größ, J., Gobbi, G. P., Di Liberto, L.,
540 Di Donfrancesco, G., Wiedensohler, A., Weingartner, E., Virtanen, A., Mentel, T. F., and Baltensperger, U.: Studying the vertical aerosol extinction coefficient by comparing in situ airborne data and elastic backscatter lidar, *Atmos. Chem. Phys.*, 16, 4539-4554, <https://doi.org/10.5194/acp-16-4539-2016>, 2016.
- Spliid, H.: Multivariate Time Series Estimation using marima. In . P. Linde (Ed.), *Symposium i anvendt statistik 2016* (pp. 108-123). Danmarks Statistik, 2016.
- 545
- Subramanian, R., Roden, C. A., Boparai. P., and Bond, T. C.: Yellow Beads and Missing Particles: Trouble Ahead for Filter-Based Absorption Measurements, *Aerosol Sci. Technol.* 41:6, 630–637, <https://doi.org/10.1080/02786820701344589>, 2007.
- 550
- Telg, H., Murphy, D. M., Bates, T. S., Johnson, J. E., Quinn, P. K., Giardi, F., and Gao, R.: A practical set of miniaturized instruments for vertical profiling of aerosol physical properties, *Aerosol Science and Technology*, 51:6, 715-723, DOI: 10.1080/02786826.2017.1296103, 2017.
- Vecchi, R., Bernardoni, V., Paganelli, C., and Valli, G.: A filter-based light-absorption measurement with polar photometer:
555 Effects of sampling artefacts from organic carbon, *Journal of Aerosol Science.*, 70, 4805-4818, <https://doi.org/10.1016/j.jaerosci.2013.12.012>, 2013.
- Wiedensohler, A., Birmili, W., Nowak, A., Sonntag, A., Weinhold, K., Merkel, M., Wehner, B., Tuch, T., Pfeifer, S., Fiebig, M., Fjåraa, A. M., Asmi, E., Sellegri, K., Depuy, R., Venzac, H., Villani, P., Laj, P., Aalto, P., Ogren, J. A., Swietlicki, E.,
560 Williams, P., Roldin, P., Quincey, P., Hüglin, C., Fierz-Schmidhauser, R., Gysel, M., Weingartner, E., Riccobono, F., Santos, S., Gröning, C., Faloon, K., Beddows, D., Harrison, R., Monahan, C., Jennings, S. G., O'Dowd, C. D., Marinoni, A., Horn, H.-



565 G., Keck, L., Jiang, J., Scheckman, J., McMurry, P. H., Deng, Z., Zhao, C. S., Moerman, M., Henzing, B., de Leeuw, G.,
Löschau, G., and Bastian, S.: Mobility particle size spectrometers: harmonization of technical standards and data structure to
facilitate high quality long-term observations of atmospheric particle number size distributions, *Atmos. Meas. Tech.*, 5, 657-
685, <https://doi.org/10.5194/amt-5-657-2012>, 2012.

World Health Organization (European Office): Health Effects of Black Carbon. Copenhagen, Denmark: WHO, ISBN:
9789289002653 2012.

570 WMO/GAW: Aerosol measurement procedures guidelines and recommendations 2nd edition, GAW Rep. 227, World
Meteorol. Organ., Geneva, Switzerland, https://library.wmo.int/doc_num.php?explnum_id=3073, 2016.

Zarzycki, C. and Bond, T. C.: How much can the vertical distribution of black carbon affect its global direct radiative forcing?,
Geophysical Research Letters - GEOPHYS RES LETT. 37. 10.1029/2010GL044555, 2010.
575



Table and figures

580

Table 1: Filter loading mass concentration (M_{eBC}) of the black carbon particles and filter areal loading density (deposited mass per spot area) $\rho_{\text{eBC},i}^*$. M_{eBC} were determined by dividing the average σ_{abs} of the STAP with an assumed MAC of $6.6 \text{ m}^2 \text{ g}^{-1}$ or based on the MAAP measurements. Usage of same filter is indicated by a separation with thick horizontal lines. Bold written entries were used for the investigation of the rh effect.

experiment	M_{eBC} [$\mu\text{g m}^{-3}$]	$\rho_{\text{eBC},i}^*$ [mg m^{-2}]	
		STAP	MA200
#1	44.5 (STAP)	14.0	5.4
	43.4 (STAP)	37.9	14.4
	27.6 (STAP)	43.0	16.3
#2	52.6 (MAAP, 2 scans)	2.9	1.1
#3	-	13.7 (integral of STAP)	no data

Table 2: Average volume and mass concentration ($V_{(\text{NH}_4)_2\text{SO}_4}$, $M_{(\text{NH}_4)_2\text{SO}_4}$) of the loading $(\text{NH}_4)_2\text{SO}_4$ aerosol derived from the used MPSS (number of used scans in brackets) and loading areal density $\rho_{(\text{NH}_4)_2\text{SO}_4}^*$ of the filters are given. Usage of same filter is indicated by a separation with thick horizontal lines, which means that the filter loading mass was adding up during the experiments.

experiment	$V_{(\text{NH}_4)_2\text{SO}_4}$ [$\mu\text{m}^3 \text{ cm}^{-3}$] (# scans)	$M_{(\text{NH}_4)_2\text{SO}_4}$ [$\mu\text{g m}^{-3}$]	$\rho_{(\text{NH}_4)_2\text{SO}_4}^*$ [mg m^{-2}]	
			STAP	MA200
#1	15.4 (2)	27.2	3.1	1.2
	18.6 (1)	32.9	10.5	4.0
	20.6 (3)	36.4	31.3	11.9
#2	20.6 (4)	36.5	40.8	15.5
	33.1 (3)	58.6	32.5	12.4
	33.5 (5)	59.3	98.7	37.6
#3	20.3 (3)	36.0	21.1	8.0
#4	20.3 (3)	36.0	41.9	15.9
#5	23.9 (3)	42.4	28.9	no data
#6	28.4 (4)	50.2	69.8	no data
#7	29.8 (2)	52.8	99.6	no data

585

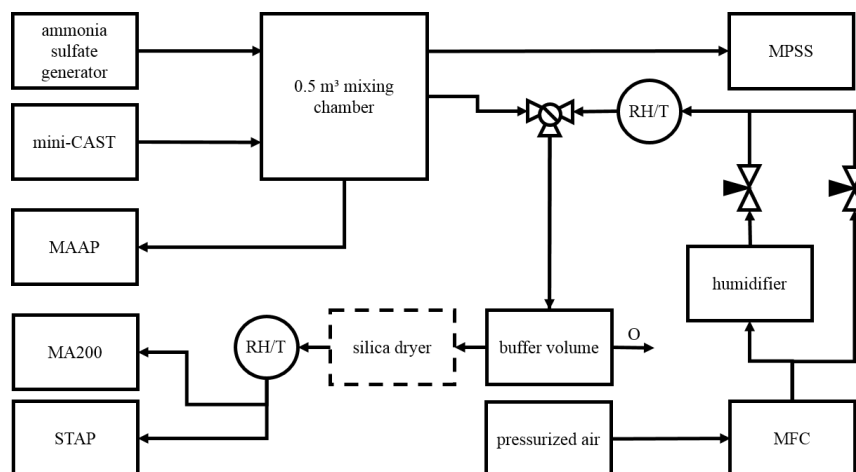


Figure 1: Scheme of the experimental setup. The volumetric flow rates of two air-streams were controlled with two needle valves to produce humidified particle free air via mixing of wet and dry particle free air. It was ensured that the sum of both flows was larger than the volumetric flow of both absorption photometer investigated here. Any exceeding airflow was directed to a buffer volume with an overflow outlet (O). The relative humidity and the temperature of the air were recorded directly after the humidifier and shortly before the photometers with the rh and T sensors.

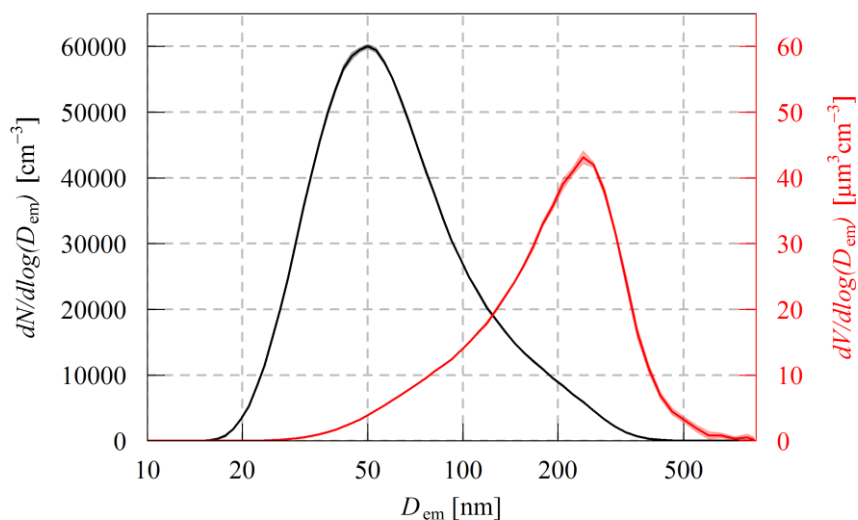


Figure 2: Average particle number (black) and volume size distributions (red) of the ammonium sulfate aerosol loaded on the filters in the MA200 and STAP during experiment #2 of the ammonium sulfate loading experiments. The average volume of $20.6 \mu\text{m}^3 \text{cm}^{-3}$ is calculated from four scans. The shaded area indicate the standard deviation of the mean. D_{em} refers herein to the electrical mobility diameter of the aerosol particles.

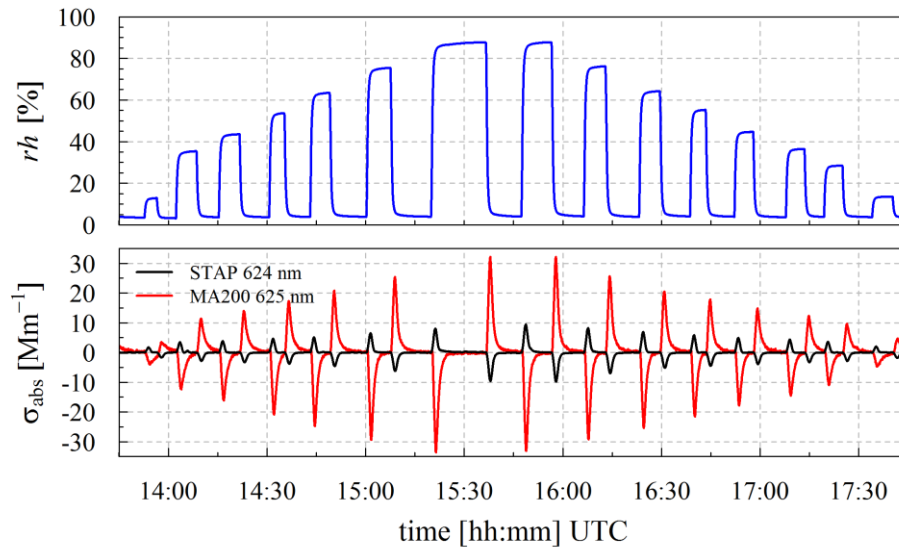


Figure 3: Time series of rh (top panel) and absorption coefficient (bottom panel) measured with STAP (624 nm; black) and MA200 (625 nm; red). Response of clean filter to fast rh changes.

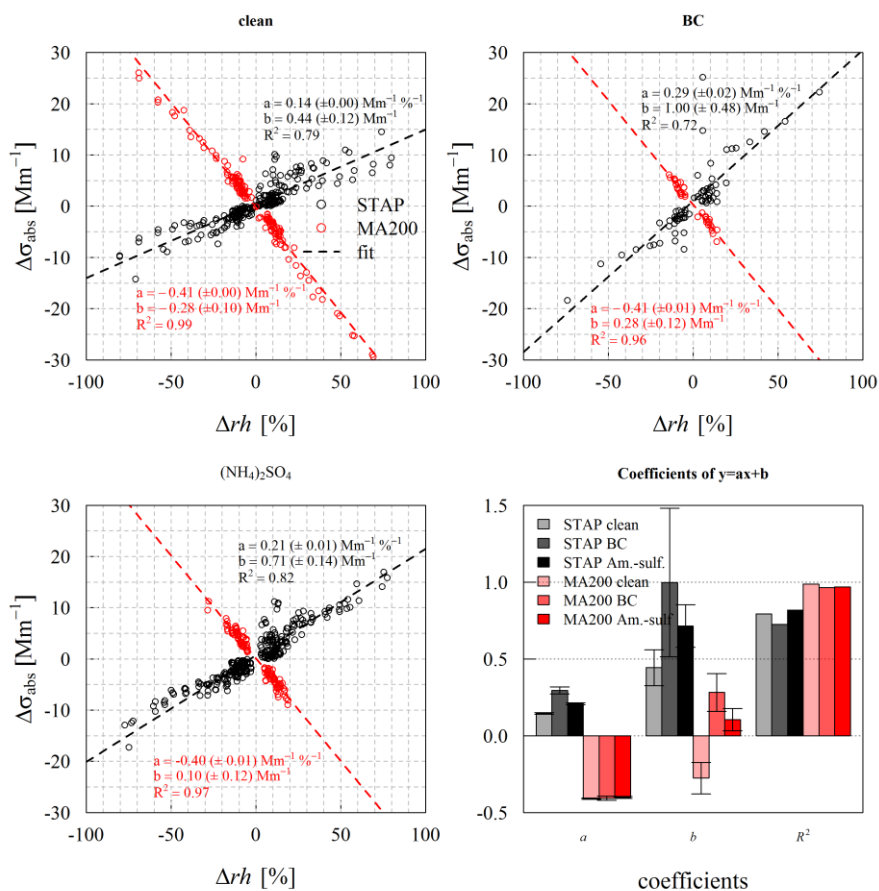


Figure 4: Scatter plot (dots) of absolute excursion of σ_{abs} ($\Delta\sigma_{\text{abs}}$) and absolute change of rh (Δrh) its linear regression fit as well as the summarizing boxplot of the linear regression fit are shown for the three investigated states at 624 nm (STAP, black colors) and 625 nm (MA200, red colors). Descriptive coefficients are given in Table B 1.

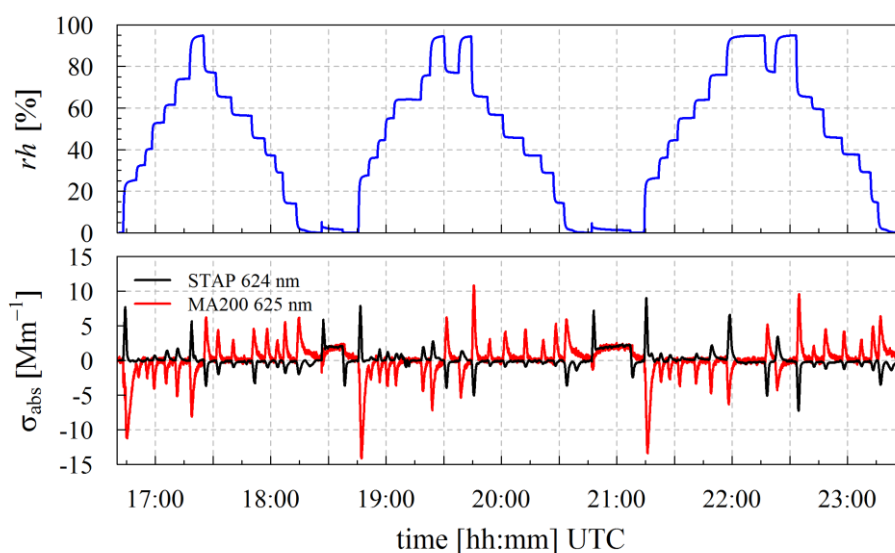


Figure 5: rh of the air stream sampled by the MA200 and the STAP (upper panel) and σ_{abs} measured by MA200 and STAP at 625 (624) nm (lower panel). First up and down ramp with clean filter, second and third loaded with ammonium.

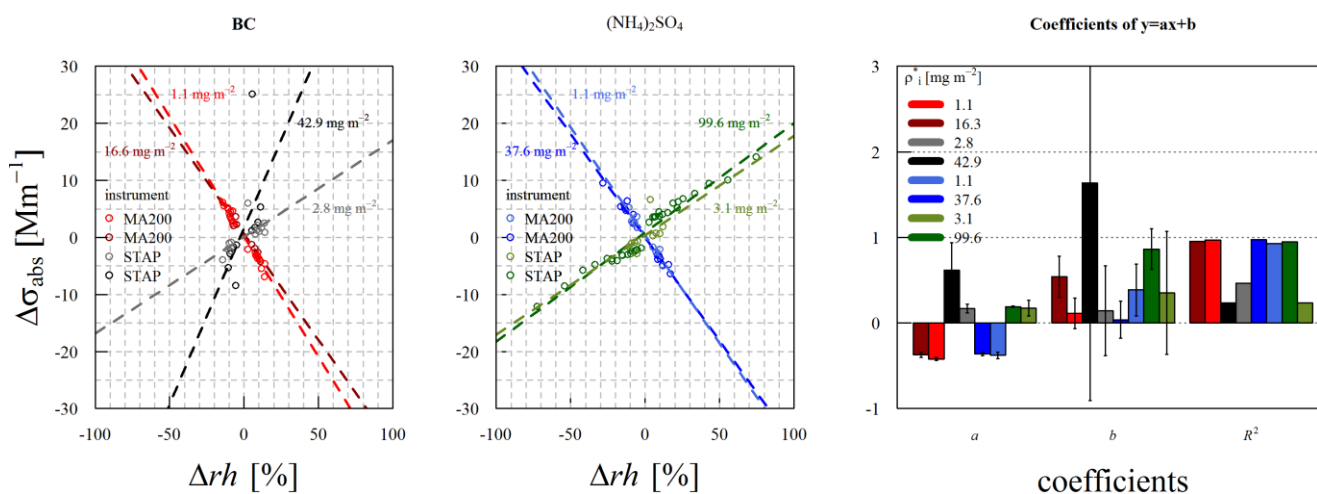


Figure 6: Scatter plot of change in absorption ($\Delta\sigma_{\text{abs}}$) over absolute change in rh (Δrh) separated into the different loading states of the filter (maximum and minimum of observed loading areal density). Red and blue colors indicate MA200 at 625 nm and black and green colors indicate STAP at 624 nm. In the first panel BC loading is shown whereas in the second panel the ammonium sulfate case is displayed. Coefficients of the linear regression fit are displayed in panel 3. Shading of color in the linear fits and of the points are same as in panel 3.

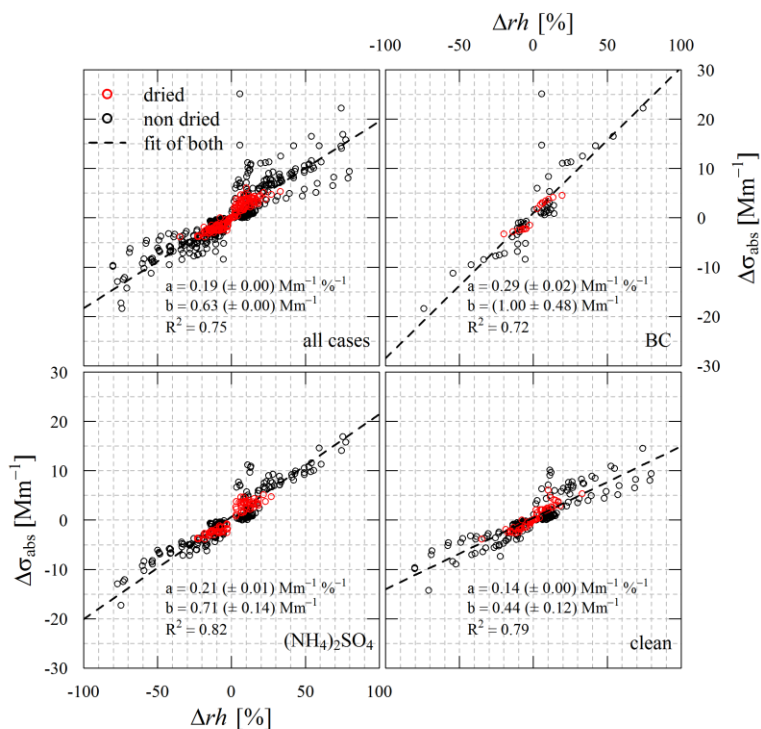


Figure 7: Change in absorption over change in rh in case for the STAP at 624 nm for all investigated points, the clean, ammonium sulfate, and BC case. Fitting coefficients of the regression lines are displayed.

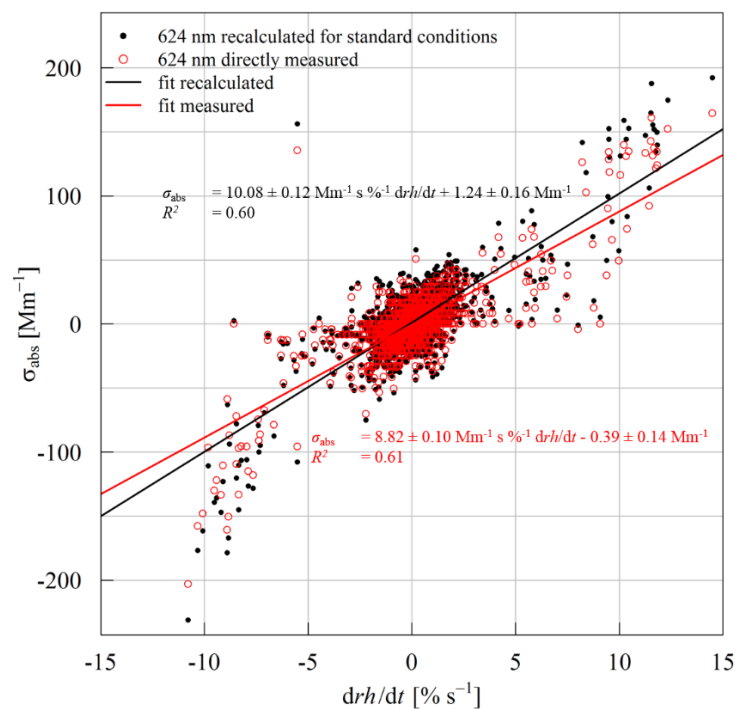


Figure 8: Scatterplot of σ_{abs} and change rate of rh (drh/dt) at 624 nm derived directly from STAP without any corrections (red) and recalculated σ_{abs} at 624 nm including corrections to standard conditions (black). Linear fit equations and correlation coefficient are given in the corresponding colors.



600

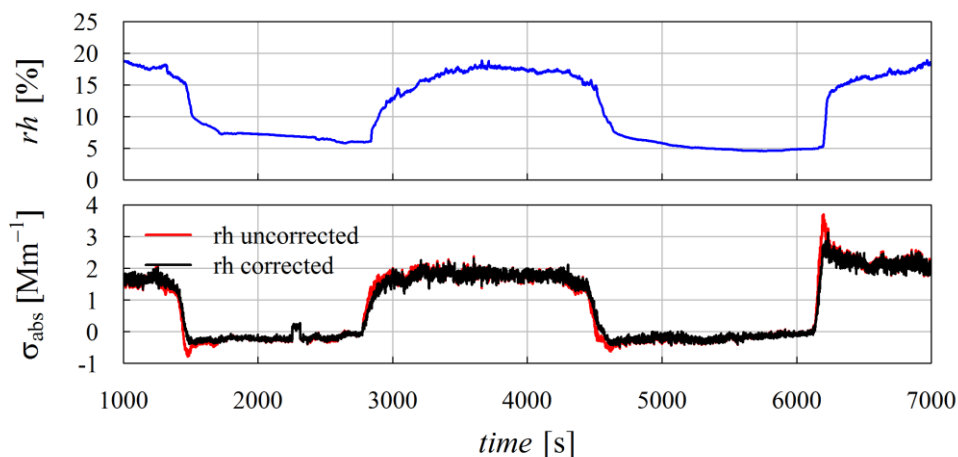


Figure 9: Time series of rh before the inlet of the STAP (blue, upper panel) and recalculated σ_{abs} (floating 60 s mean of 1 Hz calculations) at standard conditions corrected (black) and uncorrected (red) for rh changes.

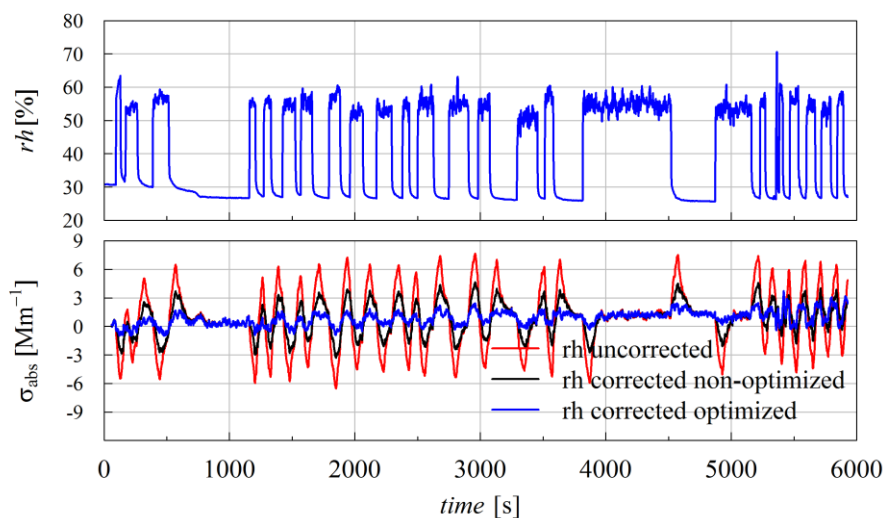


Figure 10: Time series of a laboratory measurement of σ_{abs} conducted with the MA200 without a filter. Upper panel shows the rh of the aerosol sample and the lower panel displays the 60 s floating average of measured σ_{abs} at 1 Hz time resolution and 625 nm uncorrected and biased by rh changes (red) and corrected with the modelled σ_{abs} derived with the ARMA-X model (black).